arXiv:2308.14862v1 [physics.atom-ph] 28 Aug 2023

Pinning down electron correlations in RaF via spectroscopy of excited states

M. Athanasakis-Kaklamanakis,[1,2,*] S. G. Wilkins,[3,4,†] L. V. Skripnikov,[5,‡] Á. Koszorús,[1,2] A. A. Breier,[6] M. Au,[7,8] I. Belošević,[9] R. Berger,[10] M. L. Bissell,[11] A. Borschevsky,[12] A. Brinson,[3] K. Chrysalidis,[7] T. E. Cocolios,[2] R. P. de Groote,[2] A. Dorne,[2] C. M. Fajardo-Zambrano,[2] R. W. Field,[13] K. T. Flanagan,[11,14] S. Franchoo,[15,16] R. F. Garcia Ruiz,[3,4] K. Gaul,[10] S. Geldhof,[2] T. F. Giesen,[6] D. Hanstorp,[17] R. Heinke,[7] T. A. Isaev,[5] A. A. Kyuberis,[12] S. Kujanpää,[18] L. Lalanne,[2,1] G. Neyens,[2,§] M. Nichols,[17] L. F. Pašteka,[12,19] H. A. Perrett,[11] J. R. Reilly,[11] S. Rothe,[7] S.-M. Udrescu,[3] B. van den Borne,[2] Q. Wang,[20] J. Wessolek,[11,7] X. F. Yang,[21] C. Zülch,[10] and the ISOLDE Collaboration

[1] *Experimental Physics Department, CERN, CH-1211 Geneva 23, Switzerland*
[2] *KU Leuven, Instituut voor Kern- en Stralingsfysica, B-3001 Leuven, Belgium*
[3] *Department of Physics, Massachusetts Institute of Technology, Cambridge, MA 02139, USA*
[4] *Laboratory for Nuclear Science, Massachusetts Institute of Technology, Cambridge, MA 02139, USA*
[5] *Affiliated with an institute covered by a cooperation agreement with CERN.*
[6] *Laboratory for Astrophysics, Institute of Physics, University of Kassel, Kassel 34132, Germany*
[7] *Systems Department, CERN, CH-1211 Geneva 23, Switzerland*
[8] *Department of Chemistry, Johannes Gutenberg-Universität Mainz, 55099 Mainz, Germany*
[9] *TRIUMF, Vancouver BC V6T 2A3, Canada*
[10] *Fachbereich Chemie, Philipps-Universität Marburg, Marburg 35032, Germany*
[11] *Department of Physics and Astronomy, The University of Manchester, Manchester M13 9PL, United Kingdom*
[12] *Van Swinderen Institute of Particle Physics and Gravity, University of Groningen, Groningen 9712 CP, Netherlands*
[13] *Department of Chemistry, Massachusetts Institute of Technology, Cambridge, MA 02139, USA*
[14] *Photon Science Institute, The University of Manchester, Manchester M13 9PY, United Kingdom*
[15] *Laboratoire Irène Joliot-Curie, Orsay F-91405, France*
[16] *University Paris-Saclay, Orsay F-91405, France*
[17] *Department of Physics, University of Gothenburg, Gothenburg SE-41296, Sweden*
[18] *Department of Physics, University of Jyväskylä, Jyväskylä FI-40014, Finland*
[19] *Department of Physical and Theoretical Chemistry, Faculty of Natural Sciences, Comenius University, Bratislava, Slovakia*
[20] *School of Nuclear Science and Technology, Lanzhou University, Lanzhou 730000, China*
[21] *School of Physics and State Key Laboratory of Nuclear Physics and Technology, Peking University, Beijing 100971, China*

(Dated: August 30, 2023)

We report the spectroscopy of 11 electronic states in the radioactive molecule radium monofluoride (RaF). The observed excitation energies are compared with state-of-the-art relativistic Fock-space coupled cluster (FS-RCC) calculations, which achieve an agreement of $\geq 99.71\%$ (within $\sim$8 meV) for all states. High-order electron correlation and quantum electrodynamics corrections are found to be important at all energies. Establishing the accuracy of calculations is an important step towards high-precision studies of these molecules, which are proposed for sensitive searches of physics beyond the Standard Model.

The Standard Model (SM) of particle physics fails to explain several fundamental observations, such as the matter-antimatter asymmetry and the strong charge-parity problem [1]. To reconcile the discrepancies, several theories extending beyond the Standard Model (BSM) have been proposed. To understand the limitations of the SM and to assess the validity of candidate BSM theories, precision tests of the SM and searches for new physics using atomic and molecular spectroscopy are being pursued [1] among other approaches. Such experiments typically aim to measure deviations from the SM for nuclear and hadronic symmetry-violating properties, such as the nuclear Schiff moment [2], or to detect properties that do not arise in the SM or are predicted to be significantly below the current experimental sensitivity, such as the electric dipole moment of the electron (eEDM) [3–5].

Due to the degree of precision (down to 10^{-35} e cm [6]) required by experiments aiming to perform such measurements, ongoing and future searches are focused on systems with maximum sensitivity to the presence of the various moments. Polar molecules containing a heavy and a light nucleus can have close-lying opposite-parity states and strong internal fields, thus leading to an enhanced sensitivity to the presence of symmetry-violating moments, 10^3-10^5 times larger as compared to atoms [1, 7]. HfF^+ [3] and ThO [4] are such examples, which were used to set the most stringent upper bounds to the eEDM to date at $|d_e| < 4.1 \times 10^{-30}$ e cm, while YbF [8], ThF^+ [9], BaF [10], and YbOH [11] are also being investigated, among others. Because the uncertainty in such spectroscopic searches scales with the inverse of the coherence time τ of probing each individual molecule as $\sigma \propto \frac{1}{\tau}$, radium monofluoride (RaF) is a promising system to explore the limits of the SM, as RaF is amenable

to direct laser cooling [12, 13]. Additionally, its ground state is highly sensitive to the eEDM [14–17] as well as to nuclear spin-dependent parity- or time-reversal violation (NSD-PV) [12, 18–20], depending on the chosen isotope of the octupole-deformed radium nucleus [21].

Extracting values of the symmetry-violating moments from experimental searches requires the calculation of molecular constants that quantify the sensitivity of the molecule to the moment of interest. Both in atoms and molecules [1, 22], the theoretical precision and accuracy of the calculated molecular parameters will dictate the limit to which the symmetry-violating moment can be determined. As these sensitivity parameters are not experimentally measurable, benchmarking and improving the accuracy and precision of *ab initio* molecular theory across other observables, which can be measured in the laboratory, is a critical and necessary step towards precision tests of the SM. Therefore, joint experimental and theoretical efforts should be devoted to evaluating the accuracy and precision of state-of-the-art *ab initio* methods for many different properties of the structure of RaF.

The experimental study of RaF is complicated by the radioactive decay of the radium nuclei, which all have half-lives from nanoseconds to at most a few days, except for ^{226}Ra and ^{228}Ra (years). These two long-lived isotopes have zero nuclear spin and are therefore not suited for the study of symmetry-violating nuclear moments. Radioactive ion beam (RIB) facilities are favorable not only for the preparatory spectroscopic studies needed to understand the electronic structure of the different isotopologues of RaF, but also for future precision experiments. The first spectroscopic studies on RaF molecules were performed at the ISOLDE radioactive beam facility at CERN [23]. This resulted in initial insight into the low-energy electronic-vibrational structure of RaF [24], the observation of a strong isotope shift across several short-lived isotopologues [25], and a realistic laser-cooling scheme [13].

The initial experiment and the interpretation of the data were driven by prior quantum chemistry calculations of the electronic structure of RaF [14, 26]. Subsequent theoretical studies including a higher-level treatment of electron correlations and quantum electrodynamics (QED) effects [27] suggest a re-evaluation of some of the previous assignments [24]. Furthermore, the prediction of excited-state energies and transitions with a precision of a few tens of cm^{-1} (few meV) [27, 28] call for experimental verification of the accuracy of the computational techniques.

This work reports on the experimental study of RaF by observing 11 excited electronic states up to 30,000 cm^{-1} above the ground state. The measured excitation energies are compared to state-of-the-art relativistic Fock-space coupled cluster calculations, in which corrections from QED and high-order electron correlation effects are applied to high-lying electronic states for the first time.

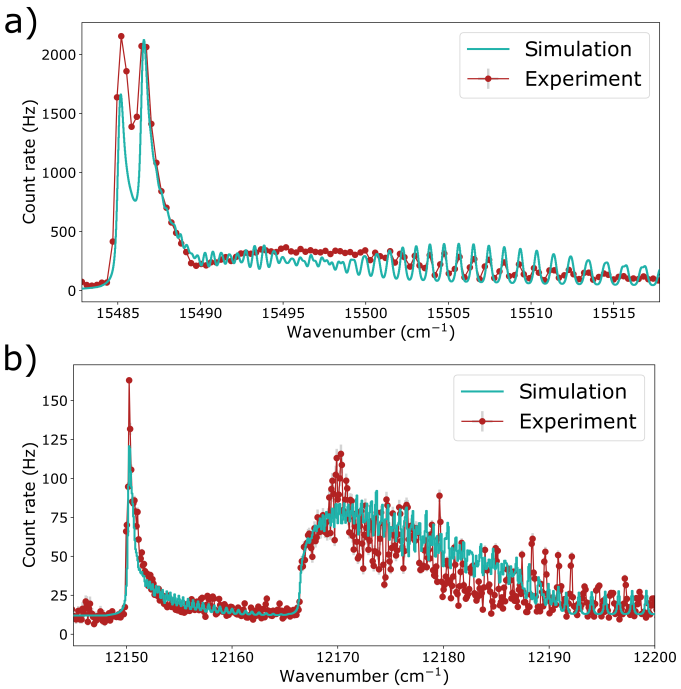

FIG. 1. Example spectra. **(a)** $G\ ^2\Pi_{1/2} \leftarrow A\ ^2\Pi_{1/2}$ ($v' = 0 \leftarrow v'' = 0$). **(b)** $E\ ^2\Sigma_{1/2} \leftarrow A\ ^2\Pi_{1/2}$ ($v' = 0 \leftarrow v'' = 0$). The simulated spectra were constructed using the best-fit molecular parameters determined using contour fitting with PGOPHER [29]. The x-axis corresponds to the wavenumber of the scanning laser.

The experimental setup is described in detail in Ref. [24] and the Supplemental Material of this Letter. Laser spectroscopy of ^{226}RaF was performed using the Collinear Resonance Ionization Spectroscopy (CRIS) experiment at CERN-ISOLDE. The delivered bunched beam of RaF$^+$ was initially neutralized via collisions with sodium vapor in a charge-exchange cell and then resonantly ionized with a series of collinear pulsed laser beams that were synchronized with the molecular bunches. For each scheme, the molecules underwent either one or two resonant excitations starting from the electronic ground state using tunable titanium-sapphire (Ti:Sa) or pulsed dye lasers (PDLs). A high-power 532-nm Nd:YAG laser was used to ionize the molecules that had been resonantly excited. The molecular excitation energies were measured by scanning the frequency of the tunable laser used for a resonant transition while monitoring the ion count rate. Example spectra are shown in Fig. 1.

The level search was facilitated by preparing multiple laser-ionization schemes based on two PDLs with nominal linewidths ν of 0.8 and 9 GHz and two grating-based broadband pulsed Ti:Sa lasers (ν = 3 GHz). A total wavenumber range of 3,935 cm^{-1} was scanned in a period of a few days. The search for excited states of the ^{226}RaF molecule was guided by theoretical pre-

dictions from relativistic Fock-space coupled cluster calculations with single- and double-excitation amplitudes (FS-RCCSD), using doubly augmented Dyall CV4Z basis sets [30, 31] and correlating 27 electrons (27e-augCV4Z) within the Dirac-Coulomb Hamiltonian. Such calculations can be completed within a few days using the DIRAC code [32, 33] and are therefore very well suited to guide the experimental efforts. Although such calculations have a limited accuracy for higher-lying states (within hundreds of cm^{-1}) it is sufficient to direct the experimental search to the correct energy range, leading to the experimental discovery of 6 new excited states (blue lines in Fig. 2).

Further information about the laser systems, measurement procedure, and data analysis can be found in the Supplemental Material.

In Fig. 2, the experimentally measured excitation energies are compared with the predictions from several *ab initio* calculations at different levels of sophistication. FS-RCCSD calculations were performed at an extended level of correlation treatment, using enhanced basis sets, and an improved electronic Hamiltonian compared to the 27e-augCV4Z calculations that guided the experiment. The excellent agreement between the observed level energies and the most advanced calculations allowed for electronic-state assignments.

To improve the treatment of electron correlations, the correlation space was expanded to include 69 electrons (triangles in Fig. 2). Including the remaining 28 electrons that correspond to the $1s$–$3d$ shells of Ra, thus correlating all 97 RaF electrons, only modified the level energies by up to 2 cm^{-1} (see Table 3 in Supplemental Material), which is significantly smaller than the overall theoretical uncertainty.

To improve the basis-set quality, calculations were performed with the extended (ext) AE3Z [34, 35] (crosses in Fig. 2) and AE4Z [28, 35] (squares in Fig. 2) basis sets, which include a greater number of functions for a more accurate description of the electronic states. A further correction for the incompleteness of the basis sets (CBS correction) was implemented based on the scalar-relativistic treatment of valence and outer-core electrons [36–38] using the CFOUR code [39] (see Supplemental Material for more details).

Finally, the accuracy of the electronic Hamiltonian was improved by taking into account the Gaunt inter-electron interaction [40] and QED effects [41], with the latter made possible recently for molecular 4-component calculations [28]. Additionally, higher-order electron correlation effects encoded in the triple-excitation amplitudes (T) were included via the FS-RCCSDT approach using the EXP-T code [42, 43]. The challenging calculation of the T contribution to the excitation energies was feasible thanks to the use of compact relativistic basis sets [34, 44, 45], developed for use with the 2-component generalized relativistic effective-core potential (GRECP) as the Hamiltonian [36–38]. The triple-excitation amplitudes were calculated for the 27 outermost electrons (correction denoted as 27e-T), including down to the $5d$ Ra electrons.

The CBS, Gaunt, QED, and 27e-T corrections are included in the diamond markers displayed in Fig. 2 and compared to the experimental excitation energies in Table I.

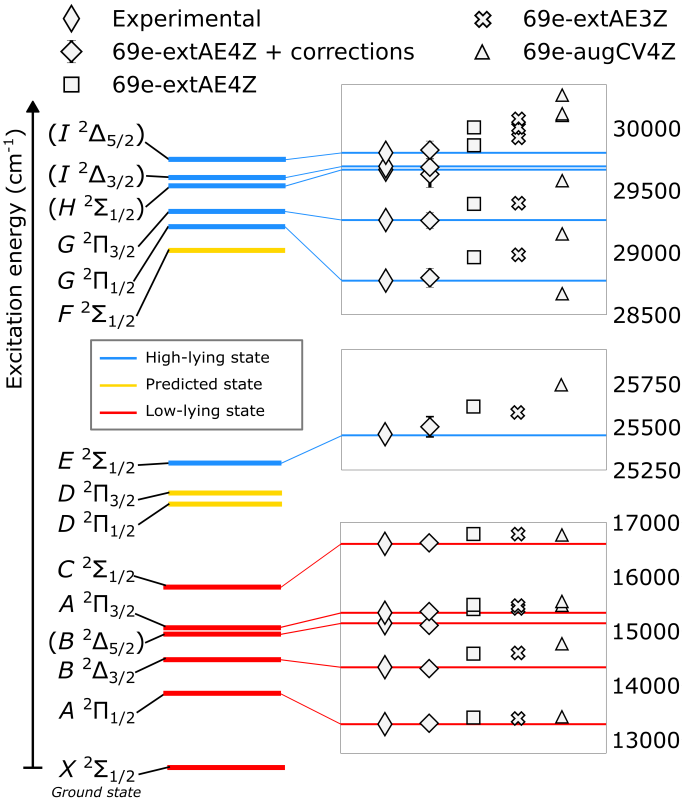

FIG. 2. **Left:** Calculated level diagram of RaF up to 30,000 cm^{-1}. The levels in red and blue have been observed experimentally, while the levels in yellow could not be searched for within the available time. The term symbols have been assigned according to the 69e-extAE4Z + corrections calculations (see text for details). **Right:** Comparison of experimental excitation energies with respect to the ground state (in cm^{-1}) and FS-RCCSD calculations at different levels of *ab initio* sophistication. Uncertainties are included only for the most precise calculations (diamonds) and in most cases are smaller than the data marker.

An overall agreement of at least 99.71% is achieved for all level energies, which allowed assigning the term characters of several states and the revision of earlier tentative assignments. A transition observed at 16,175.2(5) cm^{-1} in Ref. [24] was previously assigned as $C\ ^2\Sigma_{1/2} \leftarrow X\ ^2\Sigma_{1/2}$ ($v' = 0 \leftarrow v'' = 0$). The theoretical precision achieved in the present study together with the new measurements indicate that this transition does not correspond to the lowest electronic excitation energy of the upper state, but rather corresponds to the

($v' = 0 \leftarrow v'' = 1$) vibrational transition, as suggested in Ref. [27]. Instead, a new transition observed in this work very close to the predicted value of 16,615 cm^{-1} is identified as the $v' = 0 \leftarrow v'' = 0$ vibronic transition to the $C\ ^2\Sigma_{1/2}$ state (see Supplemental Material for details of the reassigned energy). Additionally, a transition observed at 15,142.7(5) cm^{-1} in Ref. [24] was previously tentatively assigned as ($B\ ^2\Delta_{3/2}$) $\leftarrow$ $X\ ^2\Sigma_{1/2}$ ($v' = 0 \leftarrow v'' = 0$). The close agreement of this transition energy with the calculated value of 15,099 cm^{-1} (Table I) leads to the tentative reassignment of this transition as ($B\ ^2\Delta_{5/2}$)$\leftarrow$ $X\ ^2\Sigma_{1/2}$ ($v' = 0 \leftarrow v'' = 0$). Finally, a new transition observed at 14,332.82(13)[51] cm^{-1} is closer to the theoretical prediction for the excitation energy of the $B\ ^2\Delta_{3/2}$ state, and is in agreement with the predictions in Ref. [27]. Thus, the assignment of the $B\ ^2\Delta_{3/2}$ state at 14,332.82(13)[51] cm^{-1} is adopted. The term assignments for the higher-lying states (blue lines in Fig. 2), observed in this work for the first time, are driven by the highly accurate *ab initio* calculations and elaborated upon in the Supplemental Material.

Fig. 3a and 3b present a detailed comparison of the impact of each of the corrections discussed above. In particular, the impact of treating triple-excitation amplitudes at high electronic excitation energies is clearly visible in Fig. 3b. The 27e-T correction has the most prominent effect in improving the agreement with experiment among all listed corrections and for all considered high-lying states. This correction is much larger in high-lying states (Fig. 3b) than in the low-lying ones (Fig. 3a), demonstrating the need for spectroscopic studies of electronic states far above the ground state to understand the role of correlations in the electronic structure. Fig. 3a also demonstrates the importance of choosing an appropriate basis set for calculations of excited electronic states even energetically close to the ground state, as the difference between 69e-extAE4Z and 69e-CV4Z is considerable for all states.

Finally, in Fig. 3c the impact of including QED corrections and an iterative treatment of triple-excitation amplitudes is presented. Such a study was previously performed for the low-lying states using single-reference relativistic coupled cluster theory with single, double, triple, and perturbative quadruple excitation amplitudes [46], and by including QED effects [27, 28]. The contribution of QED effects was found to be especially important for the low-lying states up to 17,000 cm^{-1} above the ground state, having a greater effect on improving the agreement with the experimental excitation energies than the iterative treatment of triple-excitation amplitudes in the FS-RCC models.

Fig. 3c confirms that the impact of QED effects is indeed significant at low energies, but it decreases in importance as the average distance of the valence electrons from the heavy Ra nucleus increases for greater excitation energies. On the other hand, the higher-order electron correlation effects captured by the iterative treatment of triple-excitation amplitudes are of increasing importance for higher-energy states, but remain non-negligible energetically close to the ground state. This is explained by the participation of non-valence outer-core electrons in the higher-energy excitations. Specifically for the excitation energies of the high-lying states, it is found that the contribution of $5d$ electrons plays a particularly important role (see Table III in Supplemental Material).

TABLE I. Comparison of experimental and theoretical electronic excitation energies (T_0, in units of cm^{-1}) in RaF. The theoretical values correspond to the 69e-extAE4Z calculations with 27e-T, CBS, Gaunt, and QED corrections (diamonds in Fig. 2). The normalized theoretical agreement (%) is reported as $1 - \frac{|E_{\rm th} - E_{\rm exp}|}{E_{\rm exp}}$. The states in parentheses are tentatively assigned. Statistical and systematic errors are given in round and square brackets.

State	Experimental	69e-extAE4Z+corr.	Agreement
$X\ ^2\Sigma_{1/2}$	0	0	
$A\ ^2\Pi_{1/2}$	13,284.427(1)[20]*	13,299(36)	**99.89**
$B\ ^2\Delta_{3/2}$	14,332.82(13)[51]**	14,300(61)	**99.77**
($B\ ^2\Delta_{5/2}$)	15,142.7(5)$^{\$}$	15,099(70)	**99.71**
$A\ ^2\Pi_{3/2}$	15,334.52(23)[35]	15,355(35)	**99.87**
$C\ ^2\Sigma_{1/2}$	16,613.6(12)$^{\#}$	16,615(69)	**99.99**
$E\ ^2\Sigma_{1/2}$	25,451.11(11)[26]	25,520(84)	**99.73**
$G\ ^2\Pi_{1/2}$	28,774.16(51)[35]	28,824(111)	**99.83**
$G\ ^2\Pi_{3/2}$	29,225.57(28)[51]	29,284(90)	**99.80**
($H\ ^2\Sigma_{1/2}$)	29,665.52(11)[51]	29,663(156)	**99.99**
($I\ ^2\Delta_{3/2}$)	29,693.15(24)[51]	29,715(102)	**99.92**
($I\ ^2\Delta_{5/2}$)	29,801.59(7)[35]	29,852(106)	**99.83**

* Value from Ref. [13].
** Previously tentatively assigned at 15,142.7(5) cm^{-1} [24].
$^{\$}$ Value from Ref. [24]. Previously tentatively assigned as $B\ ^2\Delta_{3/2}$ ($v = 0$).
$^{\#}$ Extracted using values reported in Ref. [24] following reassignment in this work. The previous assignment at 16,175.2(5) cm^{-1} [24] was deduced from a measured transition that is now reassigned as $C\ ^2\Sigma_{1/2} \leftarrow X\ ^2\Sigma_{1/2}$ ($v' = 0 \leftarrow v'' = 1$) instead of $v' = 0 \leftarrow v'' = 0$.

A highly accurate and precise treatment of electron correlation in RaF can be critical for the efforts to calculate the sensitivity of molecular electronic states to nuclear, hadronic, and leptonic symmetry-violating moments. All previous theoretical studies of the sensitivity to different symmetry-violating moments in RaF [14–17, 47–49] have reported results either using CCSD theory (with triple-excitation amplitudes included only via approximations in some works), or using the Zeroth-Order Regular Approximation based on a mean-field approach and density functional theory, which do not fully capture correlations. An investigation of the effect of high-order correlation effects on these constants is thus also needed. Moreover, the current results highlight the accuracy of the FS-RCC method, which is applicable also to molecules whose states have a multi-reference charac-

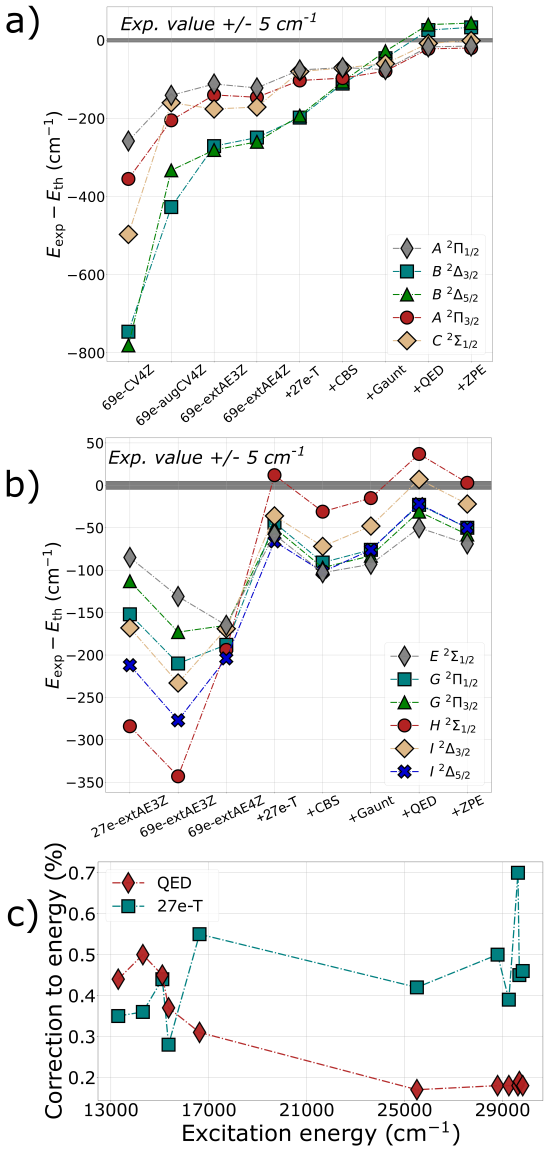

FIG. 3. Evolution of the predicted excitation energies as a function of increasing theoretical sophistication for (**a**) the five lowest-lying states and (**b**) the six high-lying states. The unambiguous identification of high-lying states through their angular momentum projections is not possible with the CV4Z basis sets and thus they are not included in (b). The '+ZPE' label corresponds to the zero-point vibrational energy correction. (**c**) Evolution of the QED and 27e-T corrections to the excitation energies calculated at the 69e-extAE4Z level.

ter, where single-reference CCSD(T) theory is not applicable.

In conclusion, Fig. 2 and Table I show that the 69e-extAE4Z calculations with 27e-T, CBS, Gaunt, and QED corrections reproduce the experimentally measured energies up to 30,000 cm^{-1} with an agreement of 99.71% or higher, which surpasses that of all previous relativistic FS-RCCSD calculations for RaF (Ref. [50] and references therein). The achieved agreement justifies the assigned angular momenta and term characters for the observed levels. Three additional states are predicted to exist (yellow lines in Fig. 2 with details in the Supplemental Material), which could not yet be identified within the available experimental time. The present study, both experimental and theoretical, paves the way for future high-resolution studies of these states and tests the predictive power of the calculations, whose reliability is a prerequisite for future precision studies and BSM probes.

SUPPLEMENTAL INFORMATION

The binned spectra that were analyzed will be available in the form of PGOPHER overlay files after publication at the reserved doi: 10.5281/zenodo.8196151. The raw data and analysis code can be provided upon request to the authors. Further information on the experimental and theoretical methods are provided in the Supplemental Material.

ACKNOWLEDGMENTS

We thank the ISOLDE collaboration and the ISOLDE technical teams for their support.

Financial support from FWO, as well as from the Excellence of Science (EOS) programme (No. 40007501) and the KU Leuven project C14/22/104, is acknowledged. The STFC consolidated grants ST/V001116/1 and ST/P004423/1 and the FNPMLS ERC grant agreement 648381 are acknowledged. SGW, RFGR, and SMU acknowledge funding by the Office of Nuclear Physics, U.S. Department of Energy Grants DE-SC0021176 and DE-SC002117. AAB, TFG, RB, and KG acknowledge funding from the Deutsche Forschungsgemeinschaft (DFG) – Projektnummer 328961117 – SFB 1319 ELCH. We thank the Center for Information Technology at the University of Groningen for their support and for providing access to the Peregrine high performance computing cluster. MAu, MN, and JW acknowledge funding from the EU's H2020-MSCA-ITN Grant No. 861198 'LISA'. DH acknowledges financial support from the Swedish Research Council (2020-03505).

DECLARATIONS

The authors declare no conflict of interest.

* m.athkak@cern.ch
† wilkinss@mit.edu
‡ skripnikov_lv@pnpi.nrcki.ru

§ gerda.neyens@kuleuven.be

[1] M. S. Safronova, D. Budker, D. DeMille, D. F. J. Kimball, A. Derevianko, and C. W. Clark, Search for new physics with atoms and molecules, Reviews of Modern Physics **90**, 10.1103/RevModPhys.90.025008 (2018).

[2] V. V. Flambaum and J. S. Ginges, Nuclear Schiff moment and time-invariance violation in atoms, Physical Review A **65**, 9 (2002).

[3] T. S. Roussy, L. Caldwell, T. Wright, W. B. Cairncross, Y. Shagam, K. B. Ng, N. Schlossberger, S. Y. Park, A. Wang, J. Ye, and E. A. Cornell, An improved bound on the electron's electric dipole moment, Science **381**, 46 (2023).

[4] V. Andreev, D. G. Ang, D. DeMille, J. M. Doyle, G. Gabrielse, J. Haefner, N. R. Hutzler, Z. Lasner, C. Meisenhelder, B. R. O'Leary, C. D. Panda, A. D. West, E. P. West, and X. Wu, Improved limit on the electric dipole moment of the electron, Nature **562**, 355 (2018).

[5] C. Cesarotti, Q. Lu, Y. Nakai, A. Parikh, and M. Reece, Interpreting the electron EDM constraint, Journal of High Energy Physics **2019**, 10.1007/JHEP05(2019)059 (2019).

[6] Y. Ema, T. Gao, and M. Pospelov, Standard model prediction for paramagnetic electric dipole moments, Phys. Rev. Lett. **129**, 231801 (2022).

[7] V. V. Flambaum and V. A. Dzuba, Electric dipole moments of atoms and molecules produced by enhanced nuclear Schiff moments, Physical Review A **101**, 042504 (2020).

[8] J. Lim, J. R. Almond, M. A. Trigatzis, J. A. Devlin, N. J. Fitch, B. E. Sauer, M. R. Tarbutt, and E. A. Hinds, Laser Cooled YbF Molecules for Measuring the Electron's Electric Dipole Moment, Physical Review Letters **120**, 123201 (2018).

[9] D. N. Gresh, K. C. Cossel, Y. Zhou, J. Ye, and E. A. Cornell, Broadband velocity modulation spectroscopy of ThF+ for use in a measurement of the electron electric dipole moment, Journal of Molecular Spectroscopy **319**, 1 (2016).

[10] P. Aggarwal, H. L. Bethlem, A. Borschevsky, M. Denis, K. Esajas, P. A. B. Haase, Y. Hao, S. Hoekstra, K. Jungmann, T. B. Meijknecht, M. C. Mooij, R. G. E. Timmermans, W. Ubachs, L. Willmann, A. Zapara, and The NL-eEDM Collaboration, Measuring the electric dipole moment of the electron in BaF, The European Physical Journal D **72**, 197 (2018).

[11] B. L. Augenbraun, Z. D. Lasner, A. Frenett, H. Sawaoka, C. Miller, T. C. Steimle, and J. M. Doyle, Laser-cooled polyatomic molecules for improved electron electric dipole moment searches, New Journal of Physics **22**, 10.1088/1367-2630/ab687b (2020).

[12] T. A. Isaev, S. Hoekstra, and R. Berger, Laser-cooled RaF as a promising candidate to measure molecular parity violation, Physical Review A - Atomic, Molecular, and Optical Physics **82**, 1 (2010).

[13] S. M. Udrescu, S. G. Wilkins, A. A. Breier, R. F. Garcia Ruiz, M. Athanasakis-Kaklamanakis, M. Au, R. Berger, I. Belosevic, M. L. Bissell, K. Chrysalidis, T. E. Cocolios, R. P. de Groote, A. Dorne, K. T. Flanagan, S. Franchoo, K. Gaul, S. Geldhof, T. F. Giesen, D. Hanstorp, R. Heinke, A. Koszorús, S. Kujanpää, L. Lalanne, G. Neyens, M. Nichols, H. A. Perrett, J. R. Reilly, S. Rothe, B. van den Borne, Q. Wang, J. Wessolek, X. F. Yang, and K. Zülch, Precision spectroscopy and laser cooling scheme of a radium-containing molecule, Under review (2023).

[14] T. A. Isaev and R. Berger, Lasercooled radium monofluoride: A molecular all-in-one probe for new physics, arXiv **1302.5682**, 10.48550/ARXIV.1302.5682 (2013).

[15] A. D. Kudashov, A. N. Petrov, L. V. Skripnikov, N. S. Mosyagin, T. A. Isaev, R. Berger, and A. V. Titov, Ab initio study of radium monofluoride (RaF) as a candidate to search for parity- and time-and-parity-violation effects, Physical Review A - Atomic, Molecular, and Optical Physics **90**, 1 (2014).

[16] S. Sasmal, H. Pathak, M. K. Nayak, N. Vaval, and S. Pal, Relativistic coupled-cluster study of RaF as a candidate for the parity- and time-reversal-violating interaction, Physical Review A **93**, 62506 (2016).

[17] C. Zhang, X. Zheng, and L. Cheng, Calculations of time-reversal-symmetry-violation sensitivity parameters based on analytic relativistic coupled-cluster gradient theory, Phys. Rev. A **104**, 012814 (2021).

[18] N. Auerbach, V. V. Flambaum, and V. Spevak, Collective T- and P-odd electromagnetic moments in nuclei with octupole deformations, Physical Review Letters **76**, 4316 (1996).

[19] V. Spevak, N. Auerbach, and V. V. Flambaum, Enhanced T-odd, P-odd electromagnetic moments in reflection asymmetric nuclei, Physical Review C - Nuclear Physics **56**, 1357 (1997).

[20] A. N. Petrov and L. V. Skripnikov, Energy levels of radium monofluoride RaF in external electric and magnetic fields to search for P- and T,P-violation effects, Phys. Rev. A **102**, 62801 (2020).

[21] P. A. Butler, L. P. Gaffney, P. Spagnoletti, K. Abrahams, M. Bowry, J. Cederkäll, G. de Angelis, H. De Witte, P. E. Garrett, A. Goldkuhle, C. Henrich, A. Illana, K. Johnston, D. T. Joss, J. M. Keatings, N. A. Kelly, M. Komorowska, J. Konki, T. Kröll, M. Lozano, B. S. Nara Singh, D. O'Donnell, J. Ojala, R. D. Page, L. G. Pedersen, C. Raison, P. Reiter, J. A. Rodriguez, D. Rosiak, S. Rothe, M. Scheck, M. Seidlitz, T. M. Shneidman, B. Siebeck, J. Sinclair, J. F. Smith, M. Stryjczyk, P. Van Duppen, S. Vinals, V. Virtanen, N. Warr, K. Wrzosek-Lipska, and M. Zielińska, Evolution of Octupole Deformation in Radium Nuclei from Coulomb Excitation of Radioactive 222Ra and 228Ra Beams, Physical Review Letters **124**, 42503 (2020).

[22] J. S. Ginges and V. V. Flambaum, Violations of fundamental symmetries in atoms and tests of unification theories of elementary particles, Physics Reports **397**, 63 (2004).

[23] R. Catherall, W. Andreazza, M. Breitenfeldt, A. Dorsival, G. J. Focker, T. P. Gharsa, G. T J, J.-L. Grenard, F. Locci, P. Martins, S. Marzari, J. Schipper, A. Shornikov, and T. Stora, The ISOLDE facility, Journal of Physics G: Nuclear and Particle Physics **44**, 094002 (2017).

[24] R. F. Garcia Ruiz, R. Berger, J. Billowes, C. L. Binnersley, M. L. Bissell, A. A. Breier, A. J. Brinson, K. Crysalidis, T. E. Cocolios, B. S. Cooper, K. T. Flanagan, T. F. Giesen, R. P. de Groote, S. Franchoo, F. P. Gustafsson, T. A. Isaev, A. Koszorus, G. Neyens, H. A. Perrett, C. M. Ricketts, S. Rothe, L. Schweikhard, A. R. Vernon, K. D. A. Wendt, F. Weinholtz, S. G. Wilkins, and X. F. Yang, Spectroscopy of short-lived radioactive molecules,

Nature **581**, 396 (2020).
[25] S. M. Udrescu, A. J. Brinson, R. F. Garcia Ruiz, K. Gaul, R. Berger, J. Billowes, C. L. Binnersley, M. L. Bissell, A. A. Breier, K. Chrysalidis, T. E. Cocolios, B. S. Cooper, K. T. Flanagan, T. F. Giesen, R. P. de Groote, S. Franchoo, F. P. Gustafsson, T. A. Isaev, A. Koszorus, G. Neyens, H. A. Perrett, C. M. Ricketts, S. Rothe, A. R. Vernon, K. D. A. Wendt, F. Wienholtz, S. G. Wilkins, and X. F. Yang, Isotope Shifts of Radium Monofluoride Molecules, Physical Review Letters **127**, 033001 (2021).
[26] T. A. Isaev, S. Hoekstra, L. Willmann, and R. Berger, Ion neutralisation mass-spectrometry route to radium monofluoride (RaF), arXiv **1310.1511**, 10.48550/ARXIV.1310.1511 (2013).
[27] A. Zaitsevskii, L. V. Skripnikov, N. S. Mosyagin, T. Isaev, R. Berger, A. A. Breier, and T. F. Giesen, Accurate ab initio calculations of RaF electronic structure appeal to more laser-spectroscopical measurements, The Journal of Chemical Physics **156**, 44306 (2022).
[28] L. V. Skripnikov, Approaching meV level for transition energies in the radium monofluoride molecule RaF and radium cation Ra+ by including quantum-electrodynamics effects, The Journal of Chemical Physics **154**, 201101 (2021).
[29] C. M. Western, PGOPHER: A program for simulating rotational, vibrational and electronic spectra, Journal of Quantitative Spectroscopy and Radiative Transfer **186**, 221 (2017).
[30] K. G. Dyall, Relativistic double-zeta, triple-zeta, and quadruple-zeta basis sets for the 4s, 5s, 6s, and 7s elements, The Journal of Physical Chemistry A **113**, 12638 (2009).
[31] K. G. Dyall, Core correlating basis functions for elements 31–118, Theor. Chem. Acc. **131**, 1217 (2012).
[32] DIRAC, a relativistic ab initio electronic structure program, Release DIRAC19 (2019), written by A. S. P. Gomes, T. Saue, L. Visscher, H. J. Aa. Jensen, and R. Bast, with contributions from I. A. Aucar, V. Bakken, K. G. Dyall, S. Dubillard, U. Ekström, E. Eliav, T. Enevoldsen, E. Faßhauer, T. Fleig, O. Fossgaard, L. Halbert, E. D. Hedegård, B. Heimlich–Paris, T. Helgaker, J. Henriksson, M. Iliaš, Ch. R. Jacob, S. Knecht, S. Komorovský, O. Kullie, J. K. Lærdahl, C. V. Larsen, Y. S. Lee, H. S. Nataraj, M. K. Nayak, P. Norman, G. Olejniczak, J. Olsen, J. M. H. Olsen, Y. C. Park, J. K. Pedersen, M. Pernpointner, R. di Remigio, K. Ruud, P. Sałek, B. Schimmelpfennig, B. Senjean, A. Shee, J. Sikkema, A. J. Thorvaldsen, J. Thyssen, J. van Stralen, M. L. Vidal, S. Villaume, O. Visser, T. Winther, and S. Yamamoto (available at http://dx.doi.org/10.5281/zenodo.3572669, see also http://www.diracprogram.org).
[33] T. Saue, R. Bast, A. S. P. Gomes, H. J. A. Jensen, L. Visscher, I. A. Aucar, R. Di Remigio, K. G. Dyall, E. Eliav, E. Fasshauer, T. Fleig, L. Halbert, E. D. Hedegård, B. Helmich-Paris, M. Iliaš, C. R. Jacob, S. Knecht, J. K. Laerdahl, M. L. Vidal, M. K. Nayak, M. Olejniczak, J. M. H. Olsen, M. Pernpointner, B. Senjean, A. Shee, A. Sunaga, and J. N. P. van Stralen, The DIRAC code for relativistic molecular calculations, J. Chem. Phys. **152**, 204104 (2020).
[34] L. V. Skripnikov, Nuclear magnetization distribution effect in molecules: Ra^+ and raf hyperfine structure, The Journal of Chemical Physics **153**, 114114 (2020).
[35] K. G. Dyall, Relativistic double-zeta, triple-zeta, and quadruple-zeta basis sets for the light elements H–Ar, Theor. Chem. Acc. **135**, 128 (2016).
[36] A. V. Titov and N. S. Mosyagin, Generalized relativistic effective core potential: Theoretical grounds, International Journal of Quantum Chemistry **71**, 359 (1999).
[37] N. S. Mosyagin, A. V. Zaitsevskii, and A. V. Titov, Shape-consistent relativistic effective potentials of small atomic cores, international review of atomic and molecular physics, Review of Atomic and Molecular Physics **1**, 63 (2010).
[38] N. S. Mosyagin, A. V. Zaitsevskii, L. V. Skripnikov, and A. V. Titov, Generalized relativistic effective core potentials for actinides, International Journal of Quantum Chemistry **116**, 301 (2016).
[39] J. F. Stanton, J. Gauss, M. E. Harding, P. G. Szalay, *et al.*, "CFOUR" (2011), CFOUR: a program package for performing high-level quantum chemical calculations on atoms and molecules, http://www.cfour.de .
[40] J. Sikkema, L. Visscher, T. Saue, and M. Iliaš, The molecular mean-field approach for correlated relativistic calculations, The Journal of Chemical Physics **131**, 124116 (2009).
[41] V. M. Shabaev, I. I. Tupitsyn, and V. A. Yerokhin, Model operator approach to the lamb shift calculations in relativistic many-electron atoms, Physical Review A **88**, 012513 (2013).
[42] A. V. Oleynichenko, A. Zaitsevskii, L. V. Skripnikov, and E. Eliav, Relativistic Fock Space Coupled Cluster Method for Many-Electron Systems: Non-Perturbative Account for Connected Triple Excitations, Symmetry **12**, 10.3390/sym12071101 (2020).
[43] A. V. Oleynichenko, A. Zaitsevskii, and E. Eliav, Towards high performance relativistic electronic structure modelling: The EXP-T program package, in *Supercomputing*, Commun. Comput. Inf. Sci., Vol. 1331, edited by V. Voevodin and S. Sobolev (Springer International Publishing, Cham, 2020) pp. 375–386.
[44] L. V. Skripnikov, N. S. Mosyagin, and A. V. Titov, Relativistic coupled-cluster calculations of spectroscopic and chemical properties for element 120, Chemical Physics Letters **555**, 79 (2013).
[45] L. V. Skripnikov, Combined 4-component and relativistic pseudopotential study of ThO for the electron electric dipole moment search, The Journal of Chemical Physics **145**, 214301 (2016).
[46] M. Kállay and J. Gauss, Approximate treatment of higher excitations in coupled-cluster theory, The Journal of Chemical Physics **123**, 214105 (2005).
[47] K. Gaul and R. Berger, Zeroth order regular approximation approach to electric dipole moment interactions of the electron, The Journal of Chemical Physics **147**, 14109 (2017).
[48] K. Gaul, S. Marquardt, T. Isaev, and R. Berger, Systematic study of relativistic and chemical enhancements of P,T-odd effects in polar diatomic radicals, Phys. Rev. A **99**, 32509 (2019).
[49] K. Gaul and R. Berger, Toolbox approach for quasirelativistic calculation of molecular properties for precision tests of fundamental physics, The Journal of Chemical Physics **152**, 044101 (2020).
[50] Y. Osika and M. Shundalau, Fock-space relativistic coupled cluster study on the RaF molecule promising for the laser cooling, Spectrochimica Acta Part A: Molecular and

Biomolecular Spectroscopy **264**, 120274 (2022).

arXiv:2308.14862v1 [physics.atom-ph] 28 Aug 2023

Supplemental Material: Pinning down electron correlations in RaF via spectroscopy of excited states

M. Athanasakis-Kaklamanakis,[1,2,*] S. G. Wilkins,[3,4,†] L. V. Skripnikov,[5,‡] Á. Koszorús,[1,2] A. A. Breier,[6] M. Au,[7,8] I. Belošević,[9] R. Berger,[10] M. L. Bissell,[11] A. Borschevsky,[12] A. Brinson,[3] K. Chrysalidis,[7] T. E. Cocolios,[2] R. P. de Groote,[2] A. Dorne,[2] C. M. Fajardo-Zambrano,[2] R. W. Field,[13] K. T. Flanagan,[11,14] S. Franchoo,[15,16] R. F. Garcia Ruiz,[3,4] K. Gaul,[10] S. Geldhof,[2] T. F. Giesen,[6] D. Hanstorp,[17] R. Heinke,[7] T. A. Isaev,[5] A. A. Kyuberis,[12] S. Kujanpää,[18] L. Lalanne,[2,1] G. Neyens,[2,§] M. Nichols,[17] L. F. Pašteka,[12,19] H. A. Perrett,[11] J. R. Reilly,[11] S. Rothe,[7] S.-M. Udrescu,[3] B. van den Borne,[2] Q. Wang,[20] J. Wessolek,[11,7] X. F. Yang,[21] C. Zülch,[10] and the ISOLDE Collaboration

[1] *Experimental Physics Department, CERN, CH-1211 Geneva 23, Switzerland*
[2] *KU Leuven, Instituut voor Kern- en Stralingsfysica, B-3001 Leuven, Belgium*
[3] *Department of Physics, Massachusetts Institute of Technology, Cambridge, MA 02139, USA*
[4] *Laboratory for Nuclear Science, Massachusetts Institute of Technology, Cambridge, MA 02139, USA*
[5] *Affiliated with an institute covered by a cooperation agreement with CERN.*
[6] *Laboratory for Astrophysics, Institute of Physics, University of Kassel, Kassel 34132, Germany*
[7] *Systems Department, CERN, CH-1211 Geneva 23, Switzerland*
[8] *Department of Chemistry, Johannes Gutenberg-Universität Mainz, 55099 Mainz, Germany*
[9] *TRIUMF, Vancouver BC V6T 2A3, Canada*
[10] *Fachbereich Chemie, Philipps-Universität Marburg, Marburg 35032, Germany*
[11] *Department of Physics and Astronomy, The University of Manchester, Manchester M13 9PL, United Kingdom*
[12] *Van Swinderen Institute of Particle Physics and Gravity, University of Groningen, Groningen 9712 CP, Netherlands*
[13] *Department of Chemistry, Massachusetts Institute of Technology, Cambridge, MA 02139, USA*
[14] *Photon Science Institute, The University of Manchester, Manchester M13 9PY, United Kingdom*
[15] *Laboratoire Irène Joliot-Curie, Orsay F-91405, France*
[16] *University Paris-Saclay, Orsay F-91405, France*
[17] *Department of Physics, University of Gothenburg, Gothenburg SE-41296, Sweden*
[18] *Department of Physics, University of Jyväskylä, Jyväskylä FI-40014, Finland*
[19] *Department of Physical and Theoretical Chemistry, Faculty of Natural Sciences, Comenius University, Bratislava, Slovakia*
[20] *School of Nuclear Science and Technology, Lanzhou University, Lanzhou 730000, China*
[21] *School of Physics and State Key Laboratory of Nuclear Physics and Technology, Peking University, Beijing 100971, China*

(Dated: August 30, 2023)

EXTENDED METHODS

Production

Accelerated beams of $^{226}RaF^+$ were produced at the CERN-ISOLDE radioactive ion beam facility [1]. Prior to the experiment, short- and long-lived radioactive isotopes, among which ^{226}Ra nuclei ($t_{1/2}$ = 1600 years), were produced by impinging 1.4-GeV protons onto a room-temperature uranium carbide target. During the experiment, the irradiated target was heated up to 2000 °C to extract the produced radionuclides from within the solid matrix. By exposing the target to a constant flow of CF_4, the radium atoms formed $^{226}Ra^{19}F$ molecules that were ionized using a rhenium surface ion source. The $^{226}RaF^+$ ions were then accelerated to 40 keV and mass-separated from other radiogenic species using two dipolar magnetic separators. The continuous, isotopically pure beam of $^{226}RaF^+$ was then accumulated in a radiofrequency quadrupolar cooler-buncher (RFQcb), which released the $^{226}RaF^+$ beam in bunches with a 5-μs temporal spread once every 20 ms. The internal temperature of the beam was cooled from ∼2000 °C to near room temperature after being trapped in the RFQcb in the presence of a helium buffer gas. A typical $^{226}RaF^+$ beam intensity of 1.2×10^6 ions per second was then sent into the CRIS beam line.

Laser setup

Multiple laser schemes were used for the spectroscopy of the excited states in RaF. The spectrum of the previously reported $A\ ^2\Pi_{1/2}$ state was measured using a grating-based titanium:sapphire (Ti:Sa) laser scanned around 752 nm (in the molecular rest frame), corresponding to the transition from the ground state. The transition from the electronic ground state to this level was then used as the first step in three-step schemes to search for the higher-lying levels (at excitation energies higher than $C\ ^2\Sigma_{1/2}$), using either its $v' = 0 \leftarrow v'' = 0$ or $v' = 1 \leftarrow v'' = 1$ vibrational transitions. In all schemes, the ionization was induced by a non-resonant excitation

driven by a 532-nm Nd:YAG laser. The excitation energies of the states $B\ ^2\Delta_{3/2}$, $A\ ^2\Pi_{3/2}$, and $C\ ^2\Sigma_{1/2}$ were re-measured with two-step schemes by scanning a pulsed dye laser around 697 nm (Pyridine 1) for the $B\ ^2\Delta_{3/2}$ state, and around 651 nm and 601 nm (DCM) for the $A\ ^2\Pi_{3/2}$ and $C\ ^2\Sigma_{1/2}$ states, followed by the 532-nm non-resonant step. The new excitation energies assigned to the low-lying states are compared to our previous assignment [2] in Table I.

The remaining states were measured using three-step laser schemes. To search for the transition to the $E\ ^2\Sigma_{1/2}$ state, the second laser step was scanned around 821 nm with a second grating-based Ti:Sa laser. For the transitions to the $G\ ^2\Pi_{1/2}$, $G\ ^2\Pi_{3/2}$, $H\ ^2\Sigma_{1/2}$, $I\ ^2\Delta_{3/2}$, and $I\ ^2\Delta_{5/2}$ states, the second laser-excitation step was scanned around 644 nm, 625 nm, 610 nm, 609 nm, and 605 nm, respectively, using a pulsed dye laser (DCM).

All lasers used in this work were pulsed. The Ti:Sa lasers were pumped by a 532-nm Nd:YAG laser operating at 1 kHz, while the pulsed dye lasers were pumped by 532-nm Nd:YAG lasers operating at 50 Hz. The non-resonant 532-nm Nd:YAG laser was operating at 50 Hz, as well. The relative timing between the laser steps was controlled by triggering the Q-switches of the pulsed lasers using a multi-channel, ultra-low-jitter clock (Quantum Composer 9528). As the excited-state lifetimes were not known for the newly discovered electronic states, all three steps were temporally overlapped. The wavelengths of the pulsed dye lasers (Spectra Physics PDL and Sirah Cobra) were measured using a HighFinesse WS6-600 wavemeter and the wavelengths of the Ti:Sa lasers were measured using a HighFinesse WSU-2 wavemeter. The WSU-2 wavemeter was continuously calibrated by monitoring at the same time the wavelength of a diode laser locked to a hyperfine peak in rubidium (Toptica DL PRO 780).

Data analysis

The measured wavenumbers in the acquired spectra were firstly Doppler-shifted to the molecular rest frame wavenumber $\tilde{\nu}$ according to the expression $\tilde{\nu} = \frac{1-\beta}{\sqrt{1-\beta^2}}\tilde{\nu}_0$, where $\beta = v/c$ with c the speed of light, and $\tilde{\nu}_0$ the wavenumber in the lab frame. The velocity of the beam was determined from their kinetic energy, which was defined by the platform voltage of the radiofrequency cooler-buncher that drifted over time between 39,905 and 39,910 kV. Fluctuations and drifts of the platform voltage were monitored by continuous measurements (1 measurement per second) of the real voltage using a calibrated potential divider (PTB PT60-2) and a digital multimeter (Agilent 34401A). The voltage measurements (precision of 10 mV at 40 kV) were then used to accurately determine the velocity of the ^{226}RaF beam for each wavenumber measurement. Following Doppler-shifting, the spectra were binned with a bin size of 3 GHz.

The binned spectra were analyzed using the contour-fitting routine of the PGOPHER package [3]. The state origin T_0, rotational constant B, centrifugal distortion constant D, spin-rotation coupling constant γ (only for Σ states), and Λ-doubling constant p (only for Π and Δ states) were varied during the fitting routine to reach agreement between simulation and experiment. Interpretation of the fitted values of B, D, γ, and p will be presented in a future publication. The fitted rotational constants B increase for higher excitation energies, which is consistent with the calculated equilibrium bond length (r_e in Table V) that decreases for higher excitation energies.

All measured spectra involved electronic transitions starting from either the $X\ ^2\Sigma_{1/2}$ or the $A\ ^2\Pi_{1/2}$ states. The molecular parameters of these two states are known from the high-resolution laser spectroscopy of the $A\ ^2\Pi_{1/2} \leftarrow X\ ^2\Sigma_{1/2}$ transition in ^{226}RaF [4]. As a result, in the present study only the properties of the upper electronic state in each spectrum were varied during each fit.

The agreement between simulated and measured spectra for the transitions starting from the electronic ground state $X\ ^2\Sigma_{1/2}$ was significantly improved if the Boltzmann population distribution of the molecular beam was substituted for the sum of Gaussian population distributions centered around different values of J. The emergence of distinct temperature groups in the ground-state population of the molecular beam is attributed to spatial aberrations in the electric potential and buffer-gas density of the RFQcb during this particular experiment, leading to the non-uniform cooling of the molecular beam.

The statistical uncertainty in the excitation energies was extracted by the standard deviation of the fitted parameter given by the contour-fitting routine of PGOPHER. The uncertainty in the raw data was the error in the count rate (y-axis) in the spectra, which was determined as the square root of the number of data points in each bin. The standard deviations of the fitted excitation energies were scaled by the square root of the reduced chi-squared of the fit $\sqrt{\chi^2_r}$.

A systematic uncertainty is considered for all excitation energies, which corresponds to the Voigt-peak linewidth set in PGOPHER to best match the observed linewidths for each spectrum, and aims to account for the propensity of the contour-fitting routine to converge to local minima, as it cannot move a simulated line by more than the set linewidth [3]. An additional component of 0.02 cm^{-1} is added to account for the combined sources of systematic error stemming from the experimental equipment (see Ref. [4]).

The best-fit values and uncertainties of the excitation energies were also obtained independently using a chi-

squared minimization code written in Python and the correlated errors were determined by inspecting the corner plots of the fitted parameters. The results of the independent fitting were consistent with the results from the PGOPHER analysis, and thus the latter are used here.

The resolution of the spectra of transitions to the $G\ ^2\Pi_{1/2}$ and $E\ ^2\Sigma_{1/2}$ states was high enough to enable an analysis using the line-fitting routine of PGOPHER, which was found to yield results in agreement with contour-fitting of the same spectra. Only contour-fitting results are included in this work for the sake of consistency.

State assignment

$A\ ^2\Pi_{3/2}$

The spectrum of the transition from the electronic ground state to $A\ ^2\Pi_{3/2}$ was measured in the region where it had been previously measured in Ref. [2]. The spectrum was obtained using a laser with a linewidth of $\nu \sim 0.8$ GHz, as compared to the linewidth of $\nu \sim 10$ GHz used in Ref. [2]. Therefore, the newly acquired spectrum was fitted to re-assign the excitation energy of the state.

Due to unexpected complications in the cooling performance of the ISCOOL RFQcb, a non-uniform temperature profile complicated the fitting of the spectrum. In addition to the molecular parameters of the $A\ ^2\Pi_{3/2}$ state, the parameters for 6 Gaussian temperature profiles were also included in the contour fitting. Each Gaussian profile had the form $e^{-b(J-J_c)^2}$, where the parameter b defined the fraction of the total molecular beam found in this temperature profile, and J_c defined the rotational quantum number around which the profile is centered. J_c thus defined the average temperature of the Gaussian profile. Thus, as per the fitted parameters, 48% of the molecules were found at 155 K, 26% at 95 K, 8% at 747 K, 5% at 685 K, 5% at 362 K, and 8% at 1527 K, yielding a weighted average of the ensemble temperature of 329 K.

$B\ ^2\Delta_{3/2}$

The spectrum of the $B\ ^2\Delta_{3/2} \leftarrow X\ ^2\Sigma_{1/2}$ transition suffered from a non-uniform temperature composition as in the case of $A\ ^2\Pi_{3/2}$. The composition of the molecular beam in terms of Gaussian profiles differed from the spectrum to the $A\ ^2\Pi_{3/2}$ state, which is consistent with an observed time dependence for the performance of the RFQcb. The best contour fit was found when using 5 Gaussian profiles. As per the fitted parameters, 34% of the beam was found at 87 K, 24% at 399 K, 23% at 1367 K, 10% at 3199 K, and 9% at 828 K, yielding a weighted average of the ensemble temperature of 820 K. This is much higher than room temperature and the average temperature in the case of $A\ ^2\Pi_{3/2}$, consistent with an intervention in the RFQcb that took place in the course of the experiment aiming to improve the uniformity of the time-of-flight profile of the ion beam. The cooling performance of the RFQcb and the resulting time-of-flight are strongly coupled.

$B\ ^2\Delta_{5/2}$

The previously measured [2] spectrum that was tentatively assigned as a transition to $B\ ^2\Delta_{3/2}$ is now tentatively reassigned as a transition to $B\ ^2\Delta_{5/2}$. This assigned excitation energy is in agreement with the theoretical prediction. The transition $B\ ^2\Delta_{5/2} \leftarrow X\ ^2\Sigma_{1/2}$ is expected to be weak but allowed by the L-uncoupling interaction of the $B\ ^2\Delta_{5/2}$ state with $A\ ^2\Pi_{3/2}$, or less likely through the electric quadrupole matrix element. Therefore, in the absence of additional information that can be used to unambiguously identify the upper state, this assignment remains tentative.

$C\ ^2\Sigma_{1/2}$

The new assignment for the energy of the $C\ ^2\Sigma_{1/2}$ state follows from the observation of a transition in close agreement with the prediction at 16,615 cm^{-1}, starting from the electronic ground state. This transition lies outside the range that was scanned in Ref. [2] and was thus not observed previously. The spectral profile of this transition is very similar to that of the transition at 16,175.2 cm^{-1} that was previously assigned as $C\ ^2\Sigma_{1/2} \leftarrow X\ ^2\Sigma_{1/2}$ ($v' = 0 \leftarrow v'' = 0$), but its intensity is twice that of the transition at 16,175.2 cm^{-1}. As a result, it is concluded that it is the newly discovered transition that in fact corresponds to $C\ ^2\Sigma_{1/2} \leftarrow X\ ^2\Sigma_{1/2}$ ($v' = 0 \leftarrow v'' = 0$).

The temperature non-uniformity due to the RFQcb led to a very complicated and noisy spectrum in this case, and the fit was not deemed as reliable as that of the spectra reported in Ref. [2]. Therefore, the new assignment for the $C\ ^2\Sigma_{1/2}$ ($v = 0$) state was determined using the values reported in Ref. [2]. The excitation energy of the $X\ ^2\Sigma_{1/2}$ $v = 1$ was determined to be $E_X(1) = 438.4(11)$ cm^{-1} by taking the difference in energy between the $A\ ^2\Pi_{1/2} \leftarrow X\ ^2\Sigma_{1/2}$ ($v' = 0 \leftarrow v'' = 1$) and ($v' = 0 \leftarrow v'' = 0$) transitions. The excitation energy $E_X(1)$ was then added to the previous assignment of 16,175.2(5) cm^{-1}, to yield 16,613.6(12) cm^{-1}.

$E\ ^2\Sigma_{1/2}$

The energy of the $E\ ^2\Sigma_{1/2}$ state was assigned based on a transition starting from $A\ ^2\Pi_{1/2}$ ($v = 0$).

Only two transitions were discovered in a range of 1,500 cm^{-1} around the predicted excitation energy of the $E\ ^2\Sigma_{1/2}$ state. The spectra of both transitions have very similar shapes and are separated by approximately 480 cm^{-1}, which matches the calculated vibrational spacing of the state (Table V). Since the transition starts from $v = 0$ of the lower state, the two measured spectra were interpreted as belonging to transitions to $v = 0$ and $v = 1$ of the $E\ ^2\Sigma_{1/2}$ state, which is the only state predicted to lie within a few thousand cm^{-1} of the measured structures.

$G\ ^2\Pi_{1/2}$

The energy of the $G\ ^2\Pi_{1/2}$ state was assigned based on a transition starting from $A\ ^2\Pi_{1/2}$ ($v = 0$).

A spectrum that starts from the same lower state as the one assigned as $G\ ^2\Pi_{1/2} \leftarrow A\ ^2\Pi_{1/2}$ ($v' = 0 \leftarrow v'' = 0$) and has a very similar spectral profile was measured at approximately 980 cm^{-1} higher in energy (corresponding to approximately two times the calculated vibrational spacing for this state, Table V), which was interpreted as a transition to $G\ ^2\Pi_{1/2}$ ($v = 2$). Additionally, in a transition starting from the $A\ ^2\Pi_{1/2}$ ($v = 1$) state, a spectrum was observed at an excitation energy half-way between those of the $v = 0$ and $v = 2$ states, with a very similar spectral profile. Therefore, this third spectrum was interpreted as belonging to a transition to $G\ ^2\Pi_{1/2}$ ($v = 1$). The intensity of the $v' = 0 \leftarrow v'' = 0$ transition was the highest, followed by that of $v' = 1 \leftarrow v'' = 1$ and then by that of the $v' = 2 \leftarrow v'' = 0$. The only other predicted state in the vicinity of $G\ ^2\Pi_{1/2}$ is $G\ ^2\Pi_{3/2}$. The transition strength of $G\ ^2\Pi_{1/2} \leftarrow A\ ^2\Pi_{1/2}$ ($v' = 0 \leftarrow v'' = 0$) was the largest among all transitions measured from $A\ ^2\Pi_{1/2}$, which is highly improbable for the nominally forbidden transition $G\ ^2\Pi_{3/2} \leftarrow A\ ^2\Pi_{1/2}$. Therefore, the observed spectrum was assigned as $G\ ^2\Pi_{1/2} \leftarrow A\ ^2\Pi_{1/2}$ ($v' = 0 \leftarrow v'' = 0$).

$G\ ^2\Pi_{3/2}$

The energy of the $G\ ^2\Pi_{3/2}$ state was assigned based on a transition starting from $A\ ^2\Pi_{1/2}$ ($v = 0$).

Within a range of 400 cm^{-1} around the prediction for the transition energy to the $G\ ^2\Pi_{3/2}$ state, spectra of two transitions were found, and the excitation energy of both would be in agreement with the prediction. However, for only one of the two transitions, a second spectrum also starting from $A\ ^2\Pi_{1/2}$ ($v = 0$) was measured at approximately 492 cm^{-1} higher in wavenumber that has a very similar spectral profile. This distance corresponds to the calculated vibrational spacing for the $G\ ^2\Pi_{3/2}$ state (Table V), and so these two spectra that had the same spectral profile were interpreted as transitions to $v = 0$ and $v = 1$ of $G\ ^2\Pi_{3/2}$.

$H\ ^2\Sigma_{1/2}$, $I\ ^2\Delta_{3/2}$, *and* $I\ ^2\Delta_{5/2}$

The energies of these three states were assigned based on transitions starting from $A\ ^2\Pi_{1/2}$ ($v = 0$).

In the vicinity of the transitions assigned to these three states, multiple transitions were observed. Two of those transitions were identified as the $v' = 1 \leftarrow v'' = 0$ and $v' = 2 \leftarrow v'' = 0$ transitions to the $G\ ^2\Pi_{3/2}$ and $G\ ^2\Pi_{1/2}$ states, respectively.

At approximately 16,175 cm^{-1}, the transition $C\ ^2\Sigma_{1/2} \leftarrow X\ ^2\Sigma_{1/2}$ ($v' = 0 \leftarrow v'' = 1$) was identified, while at approximately 16,610 cm^{-1}, the transition $C\ ^2\Sigma_{1/2} \leftarrow X\ ^2\Sigma_{1/2}$ ($v' = 0 \leftarrow v'' = 0$) was identified. These two transitions did not arise from the combined effect of all three lasers in the excitation scheme, but only from the scanning laser and the non-resonant ionization step. Therefore, they were identified as transitions from the electronic ground state, rather than from $A\ ^2\Pi_{1/2}$ ($v = 0$).

Two bands were assigned as transitions to $H\ ^2\Sigma_{1/2}$ ($v = 0$) and $I\ ^2\Delta_{3/2}$ ($v = 0$) based on the computational predictions. As the predicted energies of the two states are within uncertainties of each other, their assignment is tentative.

The spectrum that was assigned as belonging to the transition to $I\ ^2\Delta_{5/2}$ was identified due to its significantly lower intensity compared to all other spectra, which is consistent with the weak nature of the $I\ ^2\Delta_{5/2} \leftarrow A\ ^2\Pi_{1/2}$ ($v' = 0 \leftarrow v'' = 0$) transition. As the transition is dipole-forbidden, the assignment is tentative.

One more, very weak spectral feature was identified at an excitation energy of approximately 29,650 cm^{-1}, whose spectral profile suggests the form of a $\Sigma \leftarrow \Pi$ spectrum. Neither a firm nor a tentative assignment was possible at the present time. Based on the calculated T_0 and ω_e for the $F\ ^2\Sigma_{1/2}$ state, this spectrum could correspond to the transition $F\ ^2\Sigma_{1/2} \leftarrow A\ ^2\Pi_{1/2}$ ($v' = 3 \leftarrow v'' = 0$), whose strength is consistent with expected very low intensity of the observed structure. However, as no experimental information on the $F\ ^2\Sigma_{1/2}$ state has been obtained so far, a definite assignment cannot be made.

Calculations

For the 69-electron FS-RCCSD calculations, the extAE4Z basis set was used, which corresponds to the extended uncontracted Dyall's all-electron AE4Z basis set for Ra [5] from Ref. [6] and the uncontracted Dyall's AAEQZ basis set [7] for F. Explicitly, this basis set

includes $[42s\,38p\,27d\,27f\,13g\,3h\,2i]$ Gaussian-type functions for Ra. In these FS-RCCSD calculations, the energy cutoff for virtual orbitals was set equal to 300 Hartree. For the 69-electron FS-RCCSD calculations using a doubly augmented Dyall's CV4Z basis set [5, 8], the energy cutoff for virtual orbitals was set to 100 Hartree.

The electronic ground state of the RaF^+ cation (R_e = 2.165 Å) was chosen as a Fermi-vacuum in the Fock-space (FS) calculation. Target states in the neutral RaF are considered as belonging to the one-particle sector of the FS. In the calculation, the Dirac–Coulomb Hamiltonian was used to solve the self-consistent (Dirac-Hartree-Fock) problem and then converted to the two-component all-electron Hamiltonian by means of the X2C technique within the molecular mean-field approximation [9]. In addition to the 69e-FS-RCCSD-extAE4Z calculations, further calculations with different numbers of correlated electrons and utilizing different basis sets were performed. These included 27- and 69-electron calculations in the standard (unmodified) uncontracted Dyall's CV4Z basis set and 17-, 27-, 35-, 69-, and 97-electron calculations in the extended AE3Z basis set [5, 7, 8] (see Tables III and IV). The latter extAE3Z basis set has been developed in Ref. [10] and includes $[38s\,33p\,24d\,14f\,7g\,3h\,2i]$ Gaussian-type functions for Ra and corresponds to the uncontracted AE3Z [7] basis set on F.

To take into account contributions of an extended number of basis functions with high angular momentum ($L \geq 4$) beyond those contained in extAE4Z, the scalar-relativistic variant of the valence part of the generalized relativistic effective core potential approach [11–13] was used, as well as the 37e-EOMEA-CCSD approach (which is equivalent to FS-RCCSD in the considered case) to treat electron correlations using the CFOUR code [14]. In this way, it was possible to extend the basis set towards higher harmonics in Ra up to $15g\,15h\,15i$ (with an additional increase of numbers of $s\,p\,d$ functions), which is intractable in practice within the Dirac-Coulomb Hamiltonian using available resources. Following Ref. [6], the extrapolated contribution of higher harmonics to the basis-set correction was also included. In the extrapolation scheme, the contribution of basis functions with an angular momentum L (for $L > 6$) is determined using the formula $A/L^5 + B/L^6$, where the coefficients A and B were derived from the directly calculated contributions of h- (L=5) and i- (L=6) harmonics. Thus, we calculated the sum of contributions for $L > 6$. This scheme has been optimized and tested in Ref. [6] for Ra^+ and RaF excitation energies, and has also been successfully applied to calculated excitation energies in Ba^+ and BaF [15]. The contribution of the increased basis set described above is termed "+CBS" in the main text.

Correlation effects beyond the FS-RCCSD model have been calculated as the difference in transition energies calculated within the relativistic FS-RCCSDT and FS-RCCSD approaches using specially constructed compact natural contracted basis sets [10, 16, 17], correlating 27 RaF electrons and employing two-component (valence) GRECP Hamiltonian.

The compact basis is constructed in such a way as to describe the 7S, 6D, 7P, 8S, 7D, 5F and 8P states of the Ra^+ cation, which are relevant for the considered electronic states of RaF. For these states in Ra^+, scalar-relativistic 37e-CCSD(T) calculations were performed in an extended basis set, yielding correlated one-particle density matrices. The matrices were averaged and diagonalized to obtain natural atomic orbitals; in addition, functions necessary to describe spin-orbit effects were also included. Orbitals with maximal eigenvalues (occupation numbers) were used for the compact basis set in the RaF calculations. In principle, such a procedure could also be used within the Dirac-Coulomb Hamiltonian. However, at present one cannot use contracted Gaussian basis sets for heavy elements such as Ra in available implementations of the Dirac-Coulomb Hamiltonian. Another obstacle to the direct use of the Dirac-Coulomb Hamiltonian for the compact basis-set construction is the presence of serious practical limitations in the size of the original basis set that is used to construct correlated density matrices.

Lastly, the contributions of QED [6, 18] as well as Gaunt inter-electron effects [9] were calculated at the FS-RCCSD level.

In the large-scale calculations described above, we calculated differences between total energies of the excited electronic states and the ground state at the internuclear distance R = 4.23 Bohr, which is close to the equilibrium internuclear distance of the electronic ground state of RaF. However, to account for the difference in total energies at the equilibrium distance of each state, it was necessary to determine the equilibrium internuclear distances for each electronic state (Table V). The obtained "non-verticality" contributions were added to the vertical "bulk" 69-electron FS-RCCSD excitation energies obtained in the large-scale calculations. To calculate these contributions, potential energy curves for all considered electronic states were calculated.

Similarly to Ref. [19], the potential energy curve for the electronic ground state was calculated within the two-component (valence) GRECP approach using the single-reference coupled cluster with single, double and perturbative triple cluster amplitudes CCSD(T) method. To obtain potential energy curves for excited electronic states as a function of the internuclear distance R, the excitation energy calculated at the FS-RCCSD level for a given value of R was added to the energy of the electronic ground state for the same value of R. In these calculations, 37 electrons were included in the correlation treatment. For Ra, we used the $[25s\,17p\,12d\,9f\,4g\,2h]$ basis set optimized for the GRECP calculations, while for F the uncontracted Dyall's AAEQZ basis set [7] was employed.

To characterize molecular terms in the ΛS scheme, the mean values of the electron orbital angular momentum projection operator on the molecular axis were calculated at the FS-RCCSD level (within the finite-field approach) and rounded up to an integer using the code developed in Ref. [17].

In the uncertainty estimations, it is considered that the basis set correction (CBS) has an uncertainty of 50%. The calculations did not take into account the retardation part of the Breit interaction. According to the data for the Ra^+ ion [6, 20], the contribution of the retardation part of the Breit interaction to the transition energies in Ra^+ is within 20% of the Gaunt interaction effect. Thus, the uncertainty due to the excluded retardation part of the Breit interaction is estimated as 20% of the Gaunt-effect contribution. The accuracy of the model QED operator approach is high [18, 21]. Therefore, the uncertainty of the QED correction is suggested to be in the order of 20%. The uncertainty of the high-order correlation effects (beyond the FS-RCCSDT model) can be estimated by comparing the FS-RCCSDT result with the single-reference coupled cluster with single, double, triple and perturbative quadruple cluster amplitudes, CCSDT(Q) [22, 23]. According to our calculations performed for states of RaF with near single-reference character, the correlation corrections to FS-RCCSD calculated with the FS-RCCSDT and CCSDT(Q) methods agree within 60%. To be more conservative, in the uncertainty estimation it is suggested that the higher-order correlation contribution is valid within 75%. The final uncertainty estimation of the theoretical electronic excitation energies was conservatively calculated as the square root of the sum of squares of the uncertainties described above for each state.

FS-RCCSD calculations were performed using the DIRAC [24, 25] code. FS-RCCSDT calculations were performed using the using EXP-T code [26, 27]. Single reference relativistic coupled cluster calculations were performed with the MRCC [22, 23] code. All scalar relativistic correlation calculations were performed using the CFOUR [14] code. Matrix elements of the QED model Hamiltonian were calculated within the code developed in Ref. [6].

* m.athkak@cern.ch
† wilkinss@mit.edu
‡ skripnikov_lv@pnpi.nrcki.ru
§ gerda.neyens@kuleuven.be

[1] R. Catherall, W. Andreazza, M. Breitenfeldt, A. Dorsival, G. J. Focker, T. P. Gharsa, G. T J, J.-L. Grenard, F. Locci, P. Martins, S. Marzari, J. Schipper, A. Shornikov, and T. Stora, The ISOLDE facility, Journal of Physics G: Nuclear and Particle Physics **44**, 094002 (2017).

[2] R. F. Garcia Ruiz, R. Berger, J. Billowes, C. L. Binnersley, M. L. Bissell, A. A. Breier, A. J. Brinson, K. Crysalidis, T. E. Cocolios, B. S. Cooper, K. T. Flanagan, T. F. Giesen, R. P. de Groote, S. Franchoo, F. P. Gustafsson, T. A. Isaev, A. Koszorus, G. Neyens, H. A. Perrett, C. M. Ricketts, S. Rothe, L. Schweikhard, A. R. Vernon, K. D. A. Wendt, F. Weinholtz, S. G. Wilkins, and X. F. Yang, Spectroscopy of short-lived radioactive molecules, Nature **581**, 396 (2020).

[3] C. M. Western, PGOPHER: A program for simulating rotational, vibrational and electronic spectra, Journal of Quantitative Spectroscopy and Radiative Transfer **186**, 221 (2017).

[4] S. M. Udrescu, S. G. Wilkins, A. A. Breier, R. F. Garcia Ruiz, M. Athanasakis-Kaklamanakis, M. Au, R. Berger, I. Belosevic, M. L. Bissell, K. Chrysalidis, T. E. Cocolios, R. P. de Groote, A. Dorne, K. T. Flanagan, S. Franchoo, K. Gaul, S. Geldhof, T. F. Giesen, D. Hanstorp, R. Heinke, A. Koszorús, S. Kujanpää, L. Lalanne, G. Neyens, M. Nichols, H. A. Perrett, J. R. Reilly, S. Rothe, B. van den Borne, Q. Wang, J. Wessolek, X. F. Yang, and K. Zülch, Precision spectroscopy and laser cooling scheme of a radium-containing molecule, Under review (2023).

[5] K. G. Dyall, Core correlating basis functions for elements 31–118, Theor. Chem. Acc. **131**, 1217 (2012).

[6] L. V. Skripnikov, Approaching meV level for transition energies in the radium monofluoride molecule RaF and radium cation Ra+ by including quantum-electrodynamics effects, The Journal of Chemical Physics **154**, 201101 (2021).

[7] K. G. Dyall, Relativistic double-zeta, triple-zeta, and quadruple-zeta basis sets for the light elements H–Ar, Theor. Chem. Acc. **135**, 128 (2016).

[8] K. G. Dyall, Relativistic double-zeta, triple-zeta, and quadruple-zeta basis sets for the 4s, 5s, 6s, and 7s elements, The Journal of Physical Chemistry A **113**, 12638 (2009).

[9] J. Sikkema, L. Visscher, T. Saue, and M. Iliaš, The molecular mean-field approach for correlated relativistic calculations, The Journal of Chemical Physics **131**, 124116 (2009).

[10] L. V. Skripnikov, Nuclear magnetization distribution effect in molecules: Ra^+ and raf hyperfine structure, The Journal of Chemical Physics **153**, 114114 (2020).

[11] A. V. Titov and N. S. Mosyagin, Generalized relativistic effective core potential: Theoretical grounds, International Journal of Quantum Chemistry **71**, 359 (1999).

[12] N. S. Mosyagin, A. V. Zaitsevskii, and A. V. Titov, Shape-consistent relativistic effective potentials of small atomic cores, international review of atomic and molecular physics, Review of Atomic and Molecular Physics **1**, 63 (2010).

[13] N. S. Mosyagin, A. V. Zaitsevskii, L. V. Skripnikov, and A. V. Titov, Generalized relativistic effective core potentials for actinides, International Journal of Quantum Chemistry **116**, 301 (2016).

[14] J. F. Stanton, J. Gauss, M. E. Harding, P. G. Szalay, *et al.*, "CFOUR" (2011), CFOUR: a program package for performing high-level quantum chemical calculations on atoms and molecules, http://www.cfour.de .

[15] L. V. Skripnikov, D. V. Chubukov, and V. M. Shakhova, The role of qed effects in transition energies of heavy-atom alkaline earth monofluoride molecules: A theoret-

ical study of ba+, baf, raf, and e120f, J. Chem. Phys. **155**, 144103 (2021).

[16] L. V. Skripnikov, N. S. Mosyagin, and A. V. Titov, Relativistic coupled-cluster calculations of spectroscopic and chemical properties for element 120, Chemical Physics Letters **555**, 79 (2013).

[17] L. V. Skripnikov, Combined 4-component and relativistic pseudopotential study of ThO for the electron electric dipole moment search, The Journal of Chemical Physics **145**, 214301 (2016).

[18] V. M. Shabaev, I. I. Tupitsyn, and V. A. Yerokhin, Model operator approach to the lamb shift calculations in relativistic many-electron atoms, Physical Review A **88**, 012513 (2013).

[19] A. Zaitsevskii, L. V. Skripnikov, N. S. Mosyagin, T. Isaev, R. Berger, A. A. Breier, and T. F. Giesen, Accurate ab initio calculations of RaF electronic structure appeal to more laser-spectroscopical measurements, The Journal of Chemical Physics **156**, 44306 (2022).

[20] E. Eliav, U. Kaldor, and Y. Ishikawa, Transition energies of barium and radium by the relativistic coupled-cluster method, Phys. Rev. A **53**, 3050 (1996).

[21] M. Y. Kaygorodov, Y. S. Kozhedub, I. I. Tupitsyn, A. V. Malyshev, D. A. Glazov, G. Plunien, and V. M. Shabaev, Relativistic calculations of the ground and inner-l-shell excited energy levels of berylliumlike ions, Phys. Rev. A **99**, 032505 (2019).

[22] M. Kállay and J. Gauss, Approximate treatment of higher excitations in coupled-cluster theory, The Journal of Chemical Physics **123**, 214105 (2005).

[23] "MRCC", m. Kállay, P. R. Nagy, D. Mester, Z. Rolik, G. Samu, J. Csontos, J. Csóka, P. B. Szabó, L. Gyevi-Nagy, B. Hégely, I. Ladjánszki, L. Szegedy, B. Ladóczki, K. Petrov, M. Farkas, P. D. Mezei, and á. Ganyecz: The MRCC program system: Accurate quantum chemistry from water to proteins, J. Chem. Phys. 152, 074107 (2020)." "MRCC, a quantum chemical program suite written by M. Kállay, P. R. Nagy, D. Mester, Z. Rolik, G. Samu, J. Csontos, J. Csóka, P. B. Szabó, L. Gyevi-Nagy, B. Hégely, I. Ladjánszki, L. Szegedy, B. Ladóczki, K. Petrov, M. Farkas, P. D. Mezei, and á. Ganyecz. See www.mrcc.hu.

[24] DIRAC, a relativistic ab initio electronic structure program, Release DIRAC19 (2019), written by A. S. P. Gomes, T. Saue, L. Visscher, H. J. Aa. Jensen, and R. Bast, with contributions from I. A. Aucar, V. Bakken, K. G. Dyall, S. Dubillard, U. Ekström, E. Eliav, T. Enevoldsen, E. Faßhauer, T. Fleig, O. Fossgaard, L. Halbert, E. D. Hedegård, B. Heimlich–Paris, T. Helgaker, J. Henriksson, M. Iliaš, Ch. R. Jacob, S. Knecht, S. Komorovský, O. Kullie, J. K. Lærdahl, C. V. Larsen, Y. S. Lee, H. S. Nataraj, M. K. Nayak, P. Norman, G. Olejniczak, J. Olsen, J. M. H. Olsen, Y. C. Park, J. K. Pedersen, M. Pernpointner, R. di Remigio, K. Ruud, P. Sałek, B. Schimmelpfennig, B. Senjean, A. Shee, J. Sikkema, A. J. Thorvaldsen, J. Thyssen, J. van Stralen, M. L. Vidal, S. Villaume, O. Visser, T. Winther, and S. Yamamoto (available at http://dx.doi.org/10.5281/zenodo.3572669, see also http://www.diracprogram.org).

[25] T. Saue, R. Bast, A. S. P. Gomes, H. J. A. Jensen, L. Visscher, I. A. Aucar, R. Di Remigio, K. G. Dyall, E. Eliav, E. Fasshauer, T. Fleig, L. Halbert, E. D. Hedegård, B. Helmich-Paris, M. Iliaš, C. R. Jacob, S. Knecht, J. K. Laerdahl, M. L. Vidal, M. K. Nayak, M. Olejniczak, J. M. H. Olsen, M. Pernpointner, B. Senjean, A. Shee, A. Sunaga, and J. N. P. van Stralen, The DIRAC code for relativistic molecular calculations, J. Chem. Phys. **152**, 204104 (2020).

[26] A. V. Oleynichenko, A. Zaitsevskii, L. V. Skripnikov, and E. Eliav, Relativistic Fock Space Coupled Cluster Method for Many-Electron Systems: Non-Perturbative Account for Connected Triple Excitations, Symmetry **12**, 10.3390/sym12071101 (2020).

[27] A. V. Oleynichenko, A. Zaitsevskii, and E. Eliav, Towards high performance relativistic electronic structure modelling: The EXP-T program package, in *Supercomputing*, Commun. Comput. Inf. Sci., Vol. 1331, edited by V. Voevodin and S. Sobolev (Springer International Publishing, Cham, 2020) pp. 375–386.

TABLE I. Comparison of electronic excitation wavenumbers (T_0, in cm^{-1}) assigned to low-lying states in RaF between Ref. [2] and the present work. All assignments refer to the $v = 0$ vibrational state of each electronic state.

	Garcia et al. 2020	This work	Theory
$B\ ^2\Delta_{3/2}$	15,142.7(5)*	14,332.82(13)[51]	14,300(61)
$(B\ ^2\Delta_{5/2})$	—	15,142.7(5)**	15,099(70)
$A\ ^2\Pi_{3/2}$	15,344.6(50)	15,334.52(23)[35]	15,355(35)
$C\ ^2\Sigma_{1/2}$	16,175.2(5)$^{\$}$	16,613.6(12)	16,615(69)

* Tentatively assigned in Ref. [2].
** With the discovery of a state at 14,332.82(13)[51] cm^{-1}, the previously measured transition is tentatively re-interpreted in this work as $B\ ^2\Delta_{5/2} \leftarrow X\ ^2\Sigma_{1/2}$ ($v' = 0 \leftarrow v'' = 0$), bringing the tentative assignment of both levels in excellent agreement with our more accurate theoretical predictions.
$^{\$}$ Following the new measurements, this transition is re-interpreted as $C\ ^2\Sigma_{1/2} \leftarrow X\ ^2\Sigma_{1/2}$ ($v' = 0 \leftarrow v'' = 1$). Using the values reported in Ref. [2], we place the $v' = 0 \leftarrow v'' = 0$ transition at 16,613.6(12) cm^{-1}, in agreement with the theoretical prediction.

TABLE II. Theoretical adiabatic electronic excitation energies (T_e, in cm^{-1}) calculated at the 69e-FS-RCCSD-extAE4Z level including higher-order corrections. Each column presents cumulative results, adding a contribution to the values in the column to its left. In the final column, the zero-point vibrational energy is added to T_e to arrive at T_0 that is compared with experiment.

State	69e-extAE4Z	+27e-CCSDT	+CBS	+Gaunt	+QED	T_0
X $^2\Sigma_{1/2}$	0	0	0	0	0	0
A $^2\Pi_{1/2}$	13,406	13,360	13,354	13,359	13,301	13,299
B $^2\Delta_{3/2}$	14,582	14,531	14,444	14,379	14,307	14,300
B $^2\Delta_{5/2}$	15,403	15,336	15,249	15,171	15,103	15,099
A $^2\Pi_{3/2}$	15,481	15,438	15,432	15,414	15,357	15,355
C $^2\Sigma_{1/2}$	16,785	16,694	16,685	16,674	16,622	16,615
D $^2\Pi_{1/2}$	22,724	22,504	22,442	22,388	22,323	22,320
D $^2\Pi_{3/2}$	23,074	22,852	22,790	22,734	22,671	22,673
E $^2\Sigma_{1/2}$	25,616	25,509	25,554	25,544	25,501	25,520
F $^2\Sigma_{1/2}$	28,410	28,067	28,080	28,050	27,995	28,019
G $^2\Pi_{1/2}$	28,962	28,818	28,865	28,850	28,797	28,824
G $^2\Pi_{3/2}$	29,391	29,276	29,323	29,309	29,257	29,284
H $^2\Sigma_{1/2}$	29,860	29,654	29,697	29,681	29,629	29,663
I $^2\Delta_{3/2}$	29,862	29,729	29,765	29,741	29,686	29,715
I $^2\Delta_{5/2}$	30,006	29,868	29,904	29,878	29,824	29,852

TABLE III. Theoretical results (in cm^{-1}) calculated at the FS-RCCSD-extAE3Z level for different numbers of correlated electrons. Unless specified in parenthesis, the shell contributions refer to electron shells belonging to the Ra atom.

State	97e	69e	35e	27e	17e	Shell contributions			
						$1s$(F) $1s, ..., 3d$ (97e-69e)	$4s4p4d4f$ (69e-35e)	$5s5p$ (35e-27e)	$5d$ (27e-17e)
X $^2\Sigma_{1/2}$	0	0	0	0	0	0	0	0	0
A $^2\Pi_{1/2}$	13,396	13,396	13,356	13,346	13,061	0	40	10	284
B $^2\Delta_{3/2}$	14,604	14,604	14,528	14,491	14,133	0	76	37	358
B $^2\Delta_{5/2}$	15,424	15,423	15,356	15,318	14,920	0	67	38	397
A $^2\Pi_{3/2}$	15,476	15,475	15,423	15,400	15,084	2	51	24	316
C $^2\Sigma_{1/2}$	16,792	16,790	16,745	16,727	16,446	2	45	18	280
D $^2\Pi_{1/2}$	22,899	22,899	22,837	22,814	22,443	1	62	23	371
D $^2\Pi_{3/2}$	23,238	23,237	23,177	23,154	22,769	1	60	23	385
E $^2\Sigma_{1/2}$	25,582	25,582	25,542	25,536	25,208	0	40	7	328
F $^2\Sigma_{1/2}$	28,457	28,457	28,400	28,389	27,995	0	57	11	394
G $^2\Pi_{1/2}$	28,985	28,985	28,936	28,926	28,542	0	49	9	384
G $^2\Pi_{3/2}$	29,400	29,400	29,351	29,339	28,955	1	49	11	384
H $^2\Sigma_{1/2}$	30,009	30,009	29,960	29,950	29,565	0	49	10	385
I $^2\Delta_{3/2}$	29,926	29,926	29,873	29,861	29,457	0	53	13	404
I $^2\Delta_{5/2}$	30,078	30,078	30,026	30,013	29,605	0	52	13	408

TABLE IV. Theoretical electronic excitation energies (in cm^{-1}) calculated with FS-RCCSD using the CV4Z and augmented CV4Z basis sets, for 27- and 69-electron correlation spaces. The results obtained with the non-augmented CV4Z basis set could not conclusively identify the energy of the three highest-lying states in this study.

State	27e-CV4Z	69e-CV4Z	69e-augCV4Z
X $^2\Sigma_{1/2}$	0	0	0
A $^2\Pi_{1/2}$	13,517	13,542	13,425
B $^2\Delta_{3/2}$	15,009	15,079	14,770
B $^2\Delta_{5/2}$	15,856	15,924	15,478
A $^2\Pi_{3/2}$	15,648	15,690	15,549
C $^2\Sigma_{1/2}$	17,079	17,112	16,773
D $^2\Pi_{1/2}$	23,491	23,537	22,762
D $^2\Pi_{3/2}$	23,819	23,864	23,105
E $^2\Sigma_{1/2}$	26,052	26,069	25,739
F $^2\Sigma_{1/2}$	29,149	29,185	28,671
G $^2\Pi_{1/2}$	30,779	30,804	29,152
G $^2\Pi_{3/2}$	31,362	31,390	29,580
H $^2\Sigma_{1/2}$	—	—	30,105
I $^2\Delta_{3/2}$	—	—	30,118
I $^2\Delta_{5/2}$	—	—	30,268

TABLE V. Calculated equilibrium bond length and harmonic vibrational spacing for the states under 30,000 cm^{-1} from the ground state.

State	r_e ($\AA$)	ω_e (cm^{-1})
X $^2\Sigma_{1/2}$	2.24	440
A $^2\Pi_{1/2}$	2.24	435
B $^2\Delta_{3/2}$	2.25	426
B $^2\Delta_{5/2}$	2.25	430
A $^2\Pi_{3/2}$	2.24	437
C $^2\Sigma_{1/2}$	2.26	427
D $^2\Pi_{1/2}$	2.24	434
D $^2\Pi_{3/2}$	2.23	444
E $^2\Sigma_{1/2}$	2.19	481
F $^2\Sigma_{1/2}$	2.17	488
G $^2\Pi_{1/2}$	2.18	495
G $^2\Pi_{3/2}$	2.18	496
H $^2\Sigma_{1/2}$	2.18	510
I $^2\Delta_{3/2}$	2.18	497
I $^2\Delta_{5/2}$	2.18	497